ARTICLE OPEN

Check for updates

White matter microstructure alterations in early psychosis and schizophrenia

Tommaso Pavan[1]✉, Yasser Alemán-Gómez[1], Raoul Jenni[2], Pascal Steullet[2], Zoé Schilliger[2,3], Daniella Dwir[2], Martine Cleusix[2], Luis Alameda[4,5,6], Kim Q. Do[2], Philippe Conus[4], Patric Hagmann[1], Paul Klauser[2,3] and Ileana Jelescu[1]

Studies on schizophrenia feature diffusion magnetic resonance imaging (dMRI) to investigate white matter (WM) anomalies. The heterogeneity in the possible interpretations of typical Diffusion Tensor Imaging (DTI) metrics highlights the importance of increasing their specificity. Here, we characterize WM pathology in early psychosis (EP) and schizophrenia (SZ) with increased specificity using advanced dMRI: Diffusion Kurtosis Imaging and the biophysical model White Matter Tract Integrity – Watson (WMTI-W). This enables us to better characterize WM abnormalities, while preserving good sensitivity to group differences, and relate them to the current literature (ENIGMA-schizophrenia), patient's clinical characteristics and symptomatology. dMRI-derived microstructure features were extracted from all of WM and from individual regions of interest in 275 individuals. 93 subjects diagnosed with EP and 47 with SZ were compared respectively to 135 age-range matched healthy controls (HC). WM DTI diffusivities were higher, while kurtosis was lower in EP vs HC and in SZ vs HC. Differences were more widespread in EP than SZ. The regional alterations found in our cohort matched the DTI patterns found in ENIGMA-schizophrenia. WMTI-W model parameters indicate that the WM alterations in patients come primarily from the extra-axonal compartment, consistent with abnormal myelin integrity in the disease pathology. The direct link between WM alterations and symptomatology is, however, limited.

Translational Psychiatry (2025)15:179 ; https://doi.org/10.1038/s41398-025-03397-1

INTRODUCTION

Psychosis is a psychiatric disorder with heavy implications for the affected individuals, their families, and society [1]. However, the disorder etiology remains only partially understood and is considered multifactorial, involving a complex interplay of genetic, environmental, and neurobiological factors [2, 3]. Many clinical studies investigating the psychosis spectrum [4–9] reported pathological white matter (WM) as a common feature of the disease. Postmortem studies further substantiate the WM involvement found in first-episode psychosis participants [3] and in schizophrenia, reporting splitting and decompacting of myelin sheaths together with dystrophic oligodendroglia [10–13] and microglia [14].

Most in vivo studies of WM abnormalities in psychosis use diffusion magnetic resonance imaging (dMRI), an MRI technique that relies on the random motion of water molecules to explore the cellular environment and thus infer the microstructural properties of the underlying biological tissue [15]. The most popular dMRI technique in clinical research is Diffusion Tensor Imaging (DTI) and its derived scalar metrics: fractional anisotropy (FA), mean/axial/radial diffusivities (MD/AD/RD). DTI is a so-called *signal representation* [16], which means it makes no assumption about the underlying tissue and reports on the apparent diffusivity in the voxel, in any given direction of space [17].

In schizophrenia (SZ) and early psychosis (EP), the most frequently reported and accepted dMRI patterns are reduced FA and increased RD and MD [5, 8, 18–21], consistent with a loss of WM integrity and reduced diffusion barriers.

ENIGMA-schizophrenia, the largest consortium to date to coordinate an effort across multiple sites to map the WM alterations in SZ, found widespread changes with reproducible patterns across the WM in their meta-analysis [8, 22]. The most affected regions were reported to be the anterior corona radiata (ACR) and the corpus callosum [8] (CC). However, the largest effect size between patients and controls was typically found in the average WM skeleton, which seemed to drive the difference also across more specific regions of interest [8] (ROI). In early-onset psychosis, the superior longitudinal fasciculus (SLF), posterior thalamic radiation (PTR), and superior fronto-occipital fasciculus (SFO) were also reported to be affected [6]. According to the developmental interpretation of schizophrenia, alterations originate during adolescence and remain throughout the lifespan [23–26]. It is therefore expected for EP to show agreement with chronic SZ in the spatial distribution of WM alterations, albeit with reduced magnitude, as shown in Barth et al. [6].

However, while DTI metrics are sensitive to WM changes, they only provide a coarse depiction of microstructure. A first step

[1]Department of Radiology, Lausanne University Hospital (CHUV) and University of Lausanne (UNIL), Lausanne, Switzerland. [2]Center for Psychiatric Neuroscience, Department of Psychiatry, Lausanne University Hospital (CHUV) and University of Lausanne (UNIL), Lausanne, Switzerland. [3]Service of Child and Adolescent Psychiatry, Department of Psychiatry, Lausanne University Hospital (CHUV) and University of Lausanne (UNIL), Lausanne, Switzerland. [4]Service of General Psychiatry, Treatment and Early Intervention in Psychosis Program, Lausanne University Hospital (CHUV), Lausanne, Switzerland. [5]Department of Psychosis Studies, Institute of Psychiatry, Psychology and Neuroscience. King's College of London, London, UK. [6]Centro Investigacion Biomedica en Red de Salud Mental (CIBERSAM); Instituto de Biomedicina de Sevilla (IBIS), Hospital Universitario Virgen del Rocio, Departamento de Psiquiatria, Universidad de Sevilla, Sevilla, Spain. ✉email: tommaso.pavan@chuv.ch

Received: 25 April 2024 Revised: 29 April 2025 Accepted: 14 May 2025
Published online: 23 May 2025

Table 1. Overview of the effect of various pathological processes on diffusion metrics, adapted from [44].

Cellular process	Proposed changes in signal in DTI and DKI metrics	Validation experiments	Proposed changes in WMTI metrics	Validation experiments
Microgliosis	DTI ↓, DKI ↑	Early stages of the mouse cuprizone intoxication [46]	D_a ↓, $D_{e,\parallel}$ ↓, $D_{e,\perp}$ ↓	Early stages of the mouse cuprizone intoxication [46]
Astrogliosis	DTI ↓, DKI ↑	Mouse traumatic brain injury model [87]	D_a ↓, $D_{e,\parallel}$ ↓, $D_{e,\perp}$ ↓	Early stages of the mouse cuprizone intoxication [46]
Axonal swelling or beading	RD ~, MD ↓, AD ↓ ↓,RK ~, MK ↑, AK ↑ ↑	Simulation in synthetic and electron microscopy-derived mouse substrates [88, 89]	D_a ↓	Simulation of neurite beading [88]
Demyelination	RD ↑ ↑, MD ↑, AD ~,RK ↓ ↓, MK ↓, AK~	Cuprizone mouse model [46, 47, 85, 90]	f ↓, $D_{e,\parallel}$ ↑, $D_{e,\perp}$ ↑	Late stages of the mouse cuprizone intoxication [46, 47, 85]
Remyelination	RD ↓ ↓, MD ↓, AD ~,RK ↑ ↑, MK ↑, AK~	Cuprizone mouse model [46, 47]	f ↑, $D_{e,\parallel}$ ↓, $D_{e,\perp}$ ↓	Mouse cuprizone intoxication [47][a]

Astro- and microgliosis reduce water diffusivity and increase kurtosis via increased cellularity. Demyelination on the contrary translates to increased diffusivities and reduced kurtosis. When both are concomitant, they have competing effects. ↑: increase, ↓: decrease, ~: unchanged, DTI, DKI diffusion tensor and kurtosis imaging, RD, RK, MD, MK, AD, AK: Radial, Mean, Axial Diffusivity or Kurtosis, f : axonal water fraction, D_a: intra-axonal diffusivity, $D_{e,//}$, $D_{e,\perp}$:extra-axonal parallel and radial diffusivities.

[a]Opposite trends to demyelination were found for the metrics but were non-significant.

towards improving the microstructure characterization is to estimate the tissue diffusion properties more thoroughly, e.g. using Diffusion Kurtosis Imaging [27, 28] (DKI), an extension of DTI that is estimated from stronger diffusion-weighting. DKI provides complementary information about tissue heterogeneity by going beyond the Gaussian DTI approximation. DKI has been able to detect widespread WM abnormality [29] in regions with complex fiber arrangement [30], subtle abnormalities in subjects at high risk for psychosis [31] and microstructural connectivity patterns associated with processing speed deficits in SZ [32].

Nevertheless, DTI and DKI metrics are only *sensitive* to features of the tissue microstructure and their changes can be the consequence of several possible pathological mechanisms (Table 1). To gain specificity, WM *biophysical models* of diffusion are used [16], which capture the diffusion behavior in the underlying tissue with a mathematical model based on a priori knowledge of the tissue structure. Models previously used to characterize EP and SZ are free-water imaging [33] (FWI) and Neurite Orientation Dispersion and Density Imaging [34] (NODDI). Most FWI studies reported a global increase in free-water in SZ [35] and across lifespan [36]. NODDI detected decreased neurite density and increased orientation dispersion index in first-episode [37, 38] and SZ [39]. However, both models display limitations in terms of ad hoc simplifying assumptions and fit constraints (e.g. in NODDI, all three compartment diffusivities are fixed [34, 40]), strongly limiting the interpretability and validity [40] of the microstructure parameters estimated from the data [16, 41].

To overcome these limitations, we used White Matter Tract Integrity-Watson [42, 43] (WMTI-W), which enables the estimation of intra- (D_a) and extra-axonal ($D_{e,||}$, $D_{e,\perp}$) specific diffusivities that are excellent proxies for intra-axonal injury, inflammation and abnormal myelin integrity respectively [16, 43, 44], in addition to axonal density (f) and orientation dispersion (c_2). This unconstrained two-compartment model of WM has been recently used to characterize WM in a variety of pathological mechanisms (Table 1), patient populations [45] and animal models of disease [46, 47], ranging from Alzheimer's disease [48–50] to traumatic brain injury [51], but, to our knowledge, never in schizophrenia.

This work is articulated around two main hypotheses:

(i) Our Lausanne Psychosis cohort (LSP) will exhibit good consistency in WM microstructure changes characterized by DTI and DKI with the current state of the literature as reported by ENIGMA [8].

(ii) WMTI-W metrics allow the characterization of WM pathology in EP and SZ with increased specificity and limited penalty in sensitivity, as compared to the *omnibus* DTI/DKI metrics. In light of previous post-mortem ultrastructural findings of myelinated fiber pathology (myelin sheath splitting with inclusions of vacuoles, small-axons atrophy, dystrophic oligodendroglia [10–13]) and dMRI literature (widespread increased MD, RD and reduced FA [8]), we expect that our biophysical findings will be mainly reflected as increased diffusivity of the extra-axonal space and as reduced axonal density.

In an exploratory fashion, we also related WM pathology as characterized by diffusion MRI to commonly used clinical measures and characteristics, such as age of psychosis onset, illness duration, medication, and symptomatology.

METHODS

Participants

Data was collected from 135 healthy controls (HC), 93 subjects with EP and 47 with SZ (Table 2). Participants with a diagnosis of EP (within 5 years after a first psychotic episode as defined by the CAARMS [52]) or SZ (DSM-IV diagnosis of schizophrenia or schizoaffective disorder) were recruited from the Lausanne University Hospital. Exclusion criteria were psychosis related to intoxication, organic brain disease, IQ < 70, alcoholism, drug abuse, major somatic disease, or current organic brain damage. Duration of illness, age at psychosis onset, and medication were registered. HC were recruited from the same sociodemographic area of the clinical groups and were excluded if they had a first-degree family member who suffered from psychosis or prodromal symptoms, or if they reported current or past antipsychotic treatment. The HC group was further subdivided into younger (HC_{Young}, n = 130, age = 26.8 ± 6.8) and older (HC_{Old}, n = 84, age = 31.9 ± 8.1) to better match the age ranges of the two clinical groups (EP = 24.7 ± 5.5; SZ = 38.1 ± 9.4 years). Diagnoses are reported in Table S1.

MRI acquisition

MRI data was acquired on two different 3-Tesla systems (Magnetom TrioTim and PRISMA, Siemens Healthineers, Erlangen, Germany), each equipped with a 32-channel head coil. A 1-mm isotropic T1-weighted image was acquired for anatomical reference. Whole-brain diffusion-weighted images (DWI) were acquired using diffusion spectrum imaging

Table 2. Cohort demographics.

		HC_{Young} (N = 130)		HC_{Old} (N = 84)		EP (N = 93)		SZ (N = 47)		EP - HC_{Young}	SZ - HC_{Old}	EP - SZ
		Mean	SD	Mean	SD	Mean	SD	Mean	SD	p-value	p-value	p-value
Age (years)		26.8	6.8	31.9	8.1	24.7	5.5	38.1	9.4	3.0e-02*	5.6e-05****	3.5e-15****
Age at Psychosis Onset (years)						23.0	5.8	23.8	9.3			ns
Duration of illness (months)						16.3	15.5	160.8	77.9			1.3e-18****
CPZ-equivalent dose (mg/day)						341.0	274.5	319.6	287.7			ns
Delay MRI-Clin. Ass. (months)		2.5	5.5	3.1	6.9	2.1	3.2	6.6	21.3			1.0e-03**
PANSS: total						62.7	15.6	62.0	15.9			ns
PANSS: positive						7.0	2.9	8.3	3.6			2.3e-02*
PANSS: negative						14.9	5.7	14.0	5.4			ns
PANSS: disorganized						5.7	2.2	6.5	2.2			2.8e-02*
PANSS: excited						6.1	2.2	6.2	2.1			ns
PANSS: depressed						8.2	2.8	8.1	3.3			ns
GAF		83.9	4.4	83.4	4.7	56.2	11.2	56.0	13.2	1.6e-33****	4.6e-16****	ns
MADRS tot.						12.5	8.4	13.2	8.6			ns
		N	Pct.%	N	Pct.%	N	Pct.%	N	Pct.%			
Scanner	Prisma	67	51.5	43	51.2	59	63.4	20	42.6	χ^2:6.3	p = 0.096 ns	
	Trio	63	48.5	41	48.8	34	36.6	27	57.4			
Sex	Female	46	35.4	35	41.7	26	28.0	13	27.7	χ^2:4.67	p = 0.19 ns	
	Male	84	64.6	49	58.3	67	72.0	34	72.3			

HC amount to 135 Individuals, 79 HC were shared between HC_{Young} and HC_{Old}. P-values refer to Wilcoxon's tests between clinical and HC groups. χ^2 test is computed for the scanner and sex contingency table. *CPZ* chlorpromazine, *Delay MRI-Clin. Ass.* difference in months between MRI scan and clinical assessment, *GAF* global assessment of functioning, *PANSS* positive and negative syndrome scale, *MADRS* montgomery-asberg depression rating scale. *:p ≤ 5e-2, **:p ≤ 1e-2, ***:p ≤ 1e-3, ****:p ≤ 1e-4.

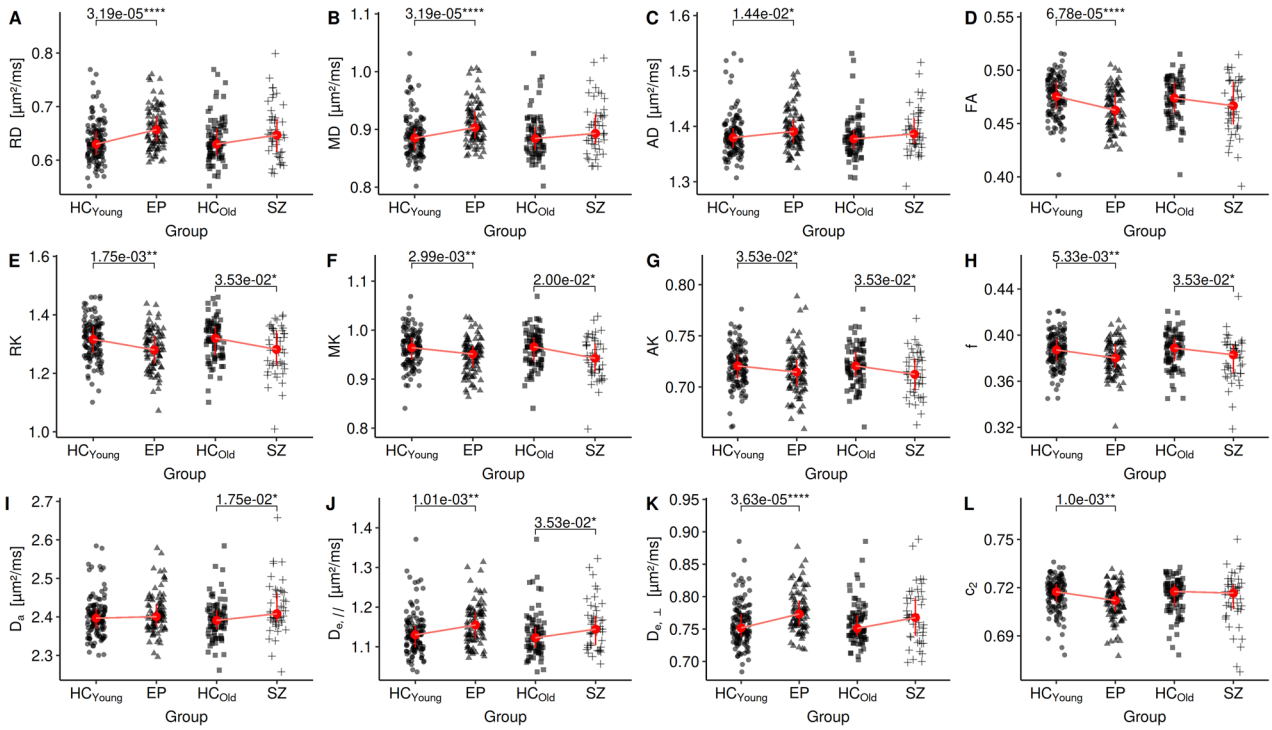

Fig. 1 Strip plot of the group comparisons. Each clinical group is compared to its respective HC group. **A**–**D**: DTI metrics, **E**–**F**: DKI metric, **H**–**L**: WMTI-W metrics. *:p ≤ 5e-2, **:p ≤ 1e-2, ***:p ≤ 1e-3, ****:p ≤ 1e-4.

(DSI) scheme across 15 b-values, ranging from 0 to 8000 s/mm^2, voxel size of $2.2 \times 2.2 \times 3$ mm^3. Further information can be found in the 'Acquisition details' section of the Supplementary Material.

Image preprocessing

The T1-weighted images were bias field corrected [53] and skull-stripped via nonlinear registration to the MNI-152 template using Advanced Normalization Tools [54] (ANTs). The diffusion preprocessing pipeline included MP-PCA denoising, Gibbs ringing-, EPI-, eddy current and motion corrections, following most recent guidelines [55]. See Supplementary Material for preprocessing details.

Microstructure estimation

For DKI and WMTI-W estimation, the diffusion dataset was truncated [27] at b ≤ 2500 s/mm^2. DKI was fitted voxel-wise [56] using Matlab, from which seven parameter maps were derived. Four from DTI: RD, MD, AD and FA, and three from DKI: radial, mean, axial kurtosis (RK, MK, AK). Then, WMTI-W model parameters were estimated voxel-wise from the DTI and DKI parameters, using an in-house Python script, yielding five additional parameter maps: axonal density f, intra-axonal diffusivity D_a, extra-axonal parallel and perpendicular diffusivities $D_{e,\parallel}$, $D_{e,\perp}$ and axon orientation alignment c_2. The WM characterization thus relied on 12 microstructure metrics. The code is available at: *github.com/Mic-map/WMTI-Watson_Python*.

ROI analysis

Individual FA maps were non-linearly registered to the Johns Hopkins University FA template [57] (JHU) using ANTs, and the WM region-of-interest (ROI) atlas labels were mapped back to individual space. The mean value of each microstructure metric was computed for each ROI, as well as in the whole-WM mask defined as the collection of all JHU ROIs (from here on referred to as 'WM core'). It should be noted that our ROI definition slightly differs from the ENIGMA ROI definition (JHU atlas intersected with the WM skeleton from TBSS analysis [58]). Our choice was guided by several factors. First, this enabled us to perform our analysis in native space instead of standard space, which reduces misalignment problems [59, 60] and completely avoids interpolation and non-linear deformations of quantitative diffusion metrics to standard space. Second, by averaging full-size ROIs instead of their intersection with the WM skeleton, we are able to study the whole volume of the WM tract instead of only the contribution of its core as defined by the maximum FA value [58]. This allows us to better account also for potential alterations at the cross-sectional boundaries/edges of the tract. Finally, our ROI definition enables us to report WM differences also in the cerebellum, an important region in schizophrenia [61], which are not reported in ENIGMA.

Psychiatric scales

Psychiatric tests included the Global Assessment of Functioning [62] scale (GAF), the Positive and Negative Syndrome Scale [63] (PANSS), and the Montgomery-Asberg Depression Rating Scale [64] (MADRS). For the PANSS, items were categorized using the Wallwork/Fortgang five-factor model [65]. PANSS data was not available for 5 EP and 1 SZ subjects, MADRS was not assessed in 6 EP and 16 SZ subjects.

Statistical analysis

Before any statistical analysis, all the microstructure parameter estimates in the WM core and individual JHU ROIs were harmonized for scanner type via ComBat harmonization [66] that was proven efficient at correcting scanner effects in the same cohort [67]. Distributions for each metric, ROI and group were tested for normality using the Shapiro–Wilk test and for homogeneity of variance using the Levene's test. The statistical test used for group comparisons was chosen based on distribution characteristics, resulting in microstructure metrics for the WM core being tested via non-parametric *Wilcoxon* signed-rank test, suitable for non-normal but homogeneous variance distributions. At the ROI level, microstructure metrics between groups were compared using the non-parametric *Brunner-Munzel* [68, 69] test, suitable for distributions with unequal variances. In all comparisons, the estimates were controlled for sex and quadratic age to properly account for age differences between groups (see 'Age correction' section in Supplementary Material, and Fig. S1). False-Discovery Rate (FDR) correction was applied to control for false positives. In total, 24 tests (12 metrics × 2 group pairs) were conducted for group differences between metrics in the WM core, and 1200 tests for ROI-specific group differences (12 metrics × 50 JHU ROIs × 2 group pairs). Finally, we tested which ROI differences would survive the inclusion of the core WM as a covariate.

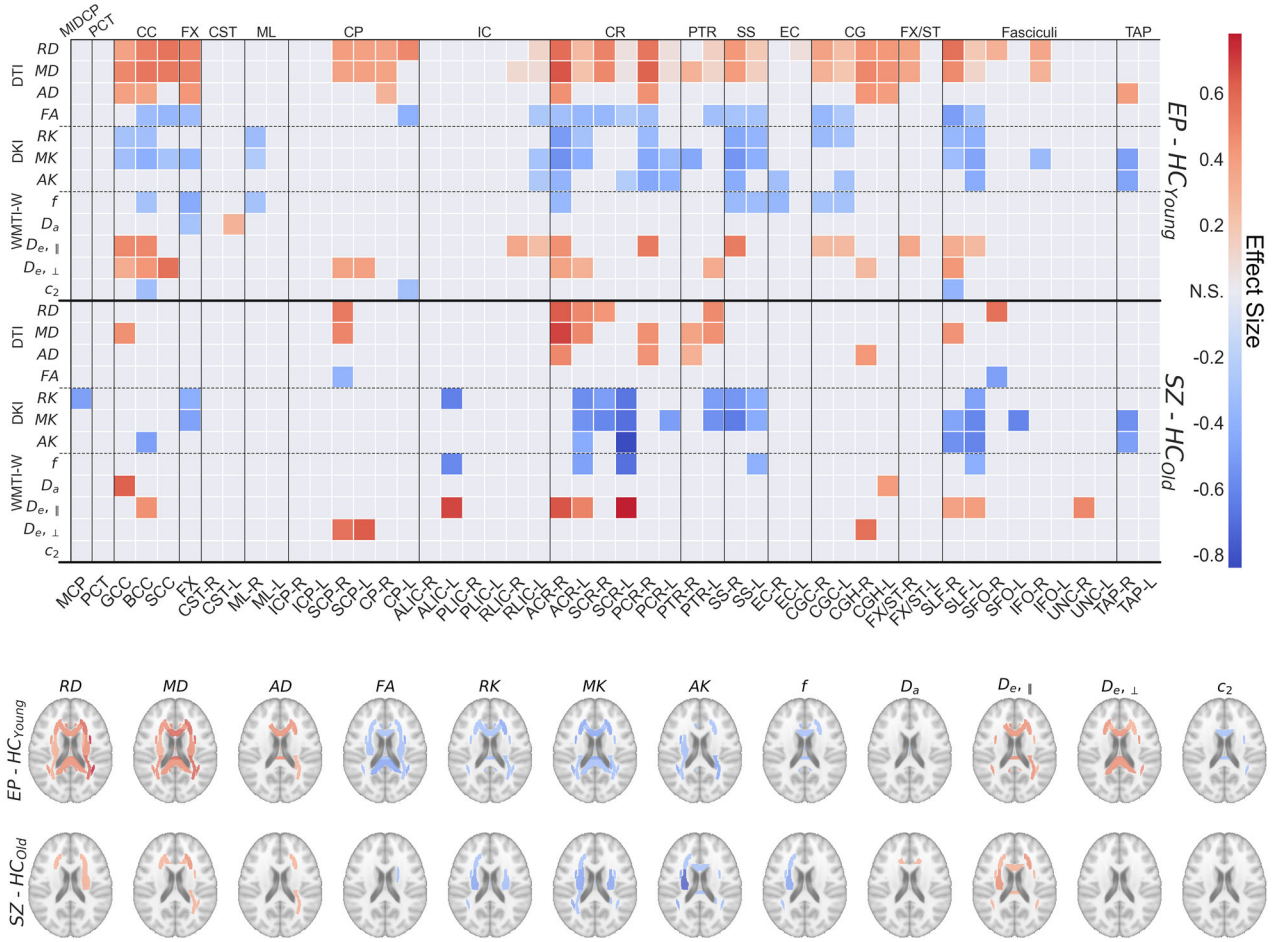

Fig. 2 Heatmaps and brainplots of the JHU ROI group comparison. Top: group comparisons (y-axis right) heatmap of the effect size, thresholded for significance, for each dMRI metric (y-axis left) and each region of interest (x-axis). Bottom: brainplots of the same comparisons. The colorbar is shared. Red: clinical group > HC, Blue: clinical group < HC. NS: $p > 0.05$, *:$p \leq 5e\text{-}2$, **:$p \leq 1e\text{-}2$, ***:$p \leq 1e\text{-}3$, ****:$p \leq 1e\text{-}4$. Numeric p-values and effect sizes can be found in Table S5, S6. *Abbreviations*: L: left; R: right; MCP: Middle cerebellar peduncle; PCT: Pontine crossing tract; GCC/BCC/SCC: Genu/Body/Splenium of corpus callosum; ; FX: Fornix (column and body); CST: Corticospinal tract; ML: Medial lemniscus; ICP/SCP: Inferior/Superior cerebellar peduncle; CP: Cerebral peduncle; ALIC/PLIC/RPIC: Anterior limb/Posterior limb/ Retrolenticular part of internal capsule; ACR/SCR/PCR: Anterior/Superior/Posterior corona radiata; PTR: Posterior thalamic radiation; SS: Sagittal stratum; EC: External capsule; CGC: Cingulum (cingulate gyrus); CGH: Cingulum (hippocampus); FX/ST: Fornix / Stria terminalis; SLF: Superior longitudinal fasciculus; SFO/IFO: Superior/Inferior fronto-occipital fasciculus; UNC: Uncinate fasciculus; TAP: Tapetum.

Effect sizes were estimated using *Cohen's d*. The dice coefficient was used to quantify the similarity in ROI alterations across the brain, indicating the proportion (between 0 and 1) of significant alterations that EP and SZ groups have in common. Agreement between effect sizes previously reported in the ENIGMA ROIs and the LSP cohort, as well as between EP vs SZ within the LSP cohort were evaluated via correlations.

Associations of the microstructure with clinical characteristics and with psychiatric scales was done via regression analysis of the 12 dMRI metrics in the WM core with age at first psychosis, duration of illness, chlorpromazine-equivalent dose (CPZ-equivalent), and psychiatric symptoms scales. They were estimated in R [70]. Each association was corrected for quadratic age and sex, and p-values were FDR corrected. Between-group differences in aging trajectories were similarly estimated, but pooling HC vs clinical participants (EP + SZ). Symptoms scale correlations were analyzed via hierarchical clustering and FDR corrected, after excluding participants with a delay between clinical assessment and MRI scan larger than 45 days, leaving 58 EP (mean delay 0.43 ± 0.60 months) and 33 SZ (0.58 ± 0.42 months).

RESULTS

Demographics

Table 2 collects cohort demographics. Age was significantly different between clinical participants and controls (i.e., EP vs HC_{Young}, $p = 0.03$; SZ vs HC_{Old}, $p < 0.0001$), hence the need for quadratic age correction. Illness duration was longer in SZ than in EP group ($p < 0.0001$).

Microstructure imaging estimates in the white matter core

Compared to HC_{Young}, EP showed significantly higher DTI diffusivities and lower FA (Fig. 1A–D; RD, MD, FA: $p < 0.0001$, AD: $p = 0.014$), as well as lower kurtosis (Fig. 1E–G; RK: $p = 0.0017$, MK: $p = 0.0029$; AK: $p = 0.035$). Axonal water fraction, f, and alignment, c_2, in EP were also significantly lower than in HC_{Young} (Fig. 1H, L; f: $p = 0.0053$, c_2: $p = 0.0010$), while extra-axonal diffusivities, $D_{e,\parallel}$ and $D_{e,\perp}$, were higher (Fig. 1J, K; $D_{e,\parallel}$: $p = 0.0010$, $D_{e,\perp}$: $p < 0.0001$). No significant differences were found in terms of intra-axonal diffusivity D_a (Fig. 1I). Effect sizes were medium to high (mean $|d| = 0.46$) with the highest being RD ($r = 0.64$), followed by FA ($r = -0.62$), MD ($r = 0.60$), and $D_{e,\perp}$ ($r = 0.59$) (Table S2).

Differences between SZ and HC_{Old} were more limited, with no significant DTI metric. Kurtosis, however, was lower in SZ (Fig. 1E–G; RK: $p = 0.035$, MK: $p = 0.020$, AK: $p = 0.035$). The WMTI-W model revealed reduced f (Fig. 1H; $p = 0.035$), increased D_a (Fig. 1I; $p = 0.017$), and $D_{e,\parallel}$ (Fig. 1J; $p = 0.035$). Effect sizes were moderate

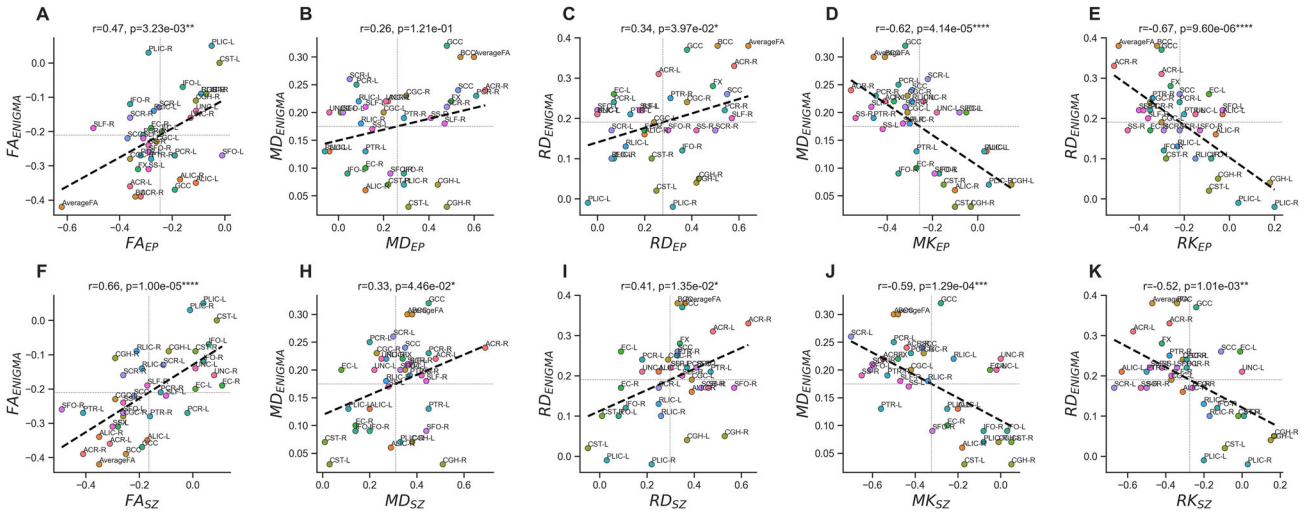

Fig. 3 ENIGMA versus Lausanne psychosis (LSP) regional effect sizes (*Cohen's d*). Plots are divided by EP (top row, **A**–**E**) and SZ (bottom row, **F**–**K**). Here, "averageWM" refers to ENIGMA average WM skeleton while for LSP it corresponds to the WM core (average of all JHU ROIs combined in one mask).

(mean $|d| = 0.38$) with the highest being MK ($r = -0.50$), followed by D_a ($r = 0.50$), RK ($r = -0.47$), and f ($r = -0.43$) (Table S3).

Microstructure imaging estimates of the white matter JHU ROIs

Group comparison of the JHU ROIs revealed distinct patterns in the microstructure metrics tendencies in both EP and SZ (Fig. 2). In EP, significant alterations in microstructure metrics were more widespread than in SZ.

DTI: In EP, MD and RD showed significant increases in 27 and 28 of the 50 ROIs, followed by lower FA in 17 ROIs. The most affected ROIs were the ACR-R ($d_{MD} = 0.65$, $d_{RD} = 0.58$), posterior CR-R (PCR, $d_{MD} = 0.61$) and SLF-R ($d_{RD} = 0.57$, $d_{FA} = -0.50$). In SZ, significant alterations were sparse, only found in 6, 8 and 2 ROIs for MD, RD and FA respectively. The most affected areas were the ACR-R ($d_{MD} = 0.69$, $d_{RD} = 0.63$), SFO-R ($d_{RD} = 0.57$, $d_{FA} = -0.49$) and right cingulum (CGH-R, $d_{MD} = 0.51$).

DKI: Kurtosis metrics were lower in both patient groups. In EP, 17 ROIs had significantly lower MK, 12 had lower RK and 10 had lower AK. The most affected ROIs were the ACR-R ($d_{MK} = -0.56$, $d_{RK} = -0.51$), the right sagittal stratum (SS-R, $d_{MK} = -0.54$, $d_{RK} = -0.45$), and right tapetum (TAP-R, $d_{MK} = -0.49$). In SZ, MK was significantly different in 12 ROIs, RK in 10 and AK in 6. The left superior CR had the highest effect size (SCR-L, $d_{AK} = -0.84$, $d_{MK} = -0.70$, and $d_{RK} = -0.67$), followed by SS-R ($d_{MK} = -0.65$) and the left anterior limb of the internal capsule (ALIC-L, $d_{RK} = -0.63$).

WMTI-W: The biophysical model attributed the changes observed in DTI and DKI metrics in EP and SZ to a reduced axonal water fraction f (in 9 and 5 ROIs, respectively) but especially higher extra-axonal diffusivities: $D_{e,\parallel}$ (in 12 and 8 ROIs) and $D_{e,\perp}$ (in 10 and 3 ROIs). In EP, the strongest effect sizes for f, $D_{e,\parallel}$ and $D_{e,\perp}$ were achieved respectively in the fornix (FX, $d_f = -0.44$), PCR-R ($d_{De,\parallel} = 0.53$), and the splenium of the CC (SCC, $d_{De,\perp} = 0.57$). For the same metrics, the SCR-L ($d_f = -0.69$, $d_{De,\parallel} = 0.78$), ALIC-L ($d_{De,\parallel} = 0.68$), the left superior cerebellar peduncle (SCP-L, $d_{De,\perp} = 0.63$) were the ROIs with highest effect size in SZ.

EP vs SZ: Overall, the Dice coefficient was 0.36, so 18 significant ROI alterations were common to both group comparisons, and we found no differences between groups. The correlation between all ROI effect sizes of EP and SZ (Fig. S2) showed strong agreement in MK and MD ($r > 0.6$) followed by RK and RD ($r = 0.55$, 0.47) and FA ($r = 0.41$). Furthermore, $D_{e,\perp}$ had stronger agreement ($r = 0.61$) than axonal water fraction f ($r = 0.41$), suggesting common features between EP and SZ as altered myelination and thus changes in the extra-axonal environment.

After covarying for the core WM, we found an increased MK, RK and decreased RD, MD in the posterior limb of the internal capsule (PLIC, $d \sim 0.40$) of EP and an increase of the ACR-R MD in SZ.

All the ordered ROI effect sizes for DTI, DKI and WMTI-W can be found in Table S4, while a 3D render of the alteration frequency can be found in Fig. S4, 5.

Regional agreement between effect sizes of ENIGMA and Lausanne Psychosis cohort

We evaluated the regional effect sizes found in DTI and DKI metrics for the two groups of our LSP cohort against the regional effect sizes in the meta-analysis by Kelly et al. [8], where only effect sizes for FA, MD, and RD were reported (Fig. 3). It is noteworthy that the ENIGMA meta-analysis reports mainly on SZ. Overall, the agreement depended on the metric and group in question. Regional FA effect size correlations between ENIGMA and LSP were stronger in SZ ($r = 0.66$, Fig. 3F) than EP ($r = 0.47$, Fig. 3A). The regional agreement of MD (Fig. 3B, H) and RD (Fig. 3C, I) was low-moderate ($0.26 < r < 0.41$). Instead, MK and RK in the LSP cohort showed the strongest associations ($0.52 < r < 0.67$) when compared to ENIGMA MD (Fig. 3D, J) and RD effect sizes (Fig. 3E, K), respectively.

Signal representations versus biophysical model: sensitivity versus specificity

Signal representations (DTI, DKI) yielded a higher number of significant differences between groups than WMTI-W metrics. When averaging regional effect sizes in significant ROIs, in EP (Fig. 4A), MK and AD had the strongest effect sizes ($|d_{ep}| = 0.40$), followed by $D_{e,\perp}$ ($d_{ep} = 0.38$). In SZ (Fig. 4B), the highest effect sizes were achieved by metrics beyond DTI: $D_{e,\perp}$ ($d_{sz} = 0.59$), AK ($d_{sz} = -0.57$), and MK ($d_{sz} = -0.56$). However, the larger number of significant ROIs in DTI may bias this result. Remarkably though, even when averaging regional effect sizes irrespective of their significance (Fig. S3), MK was the metric achieving the highest absolute effect size in SZ ($d_{sz} = -0.28$), over RD ($d_{sz} = 0.26$) and MD ($d_{sz} = 0.27$). Finally, while signal representations (DTI/DKI) are more sensitive to WM changes than biophysical model parameters (WMTI-W), it is noteworthy that the effect sizes between the two families of features are not dramatically different, while

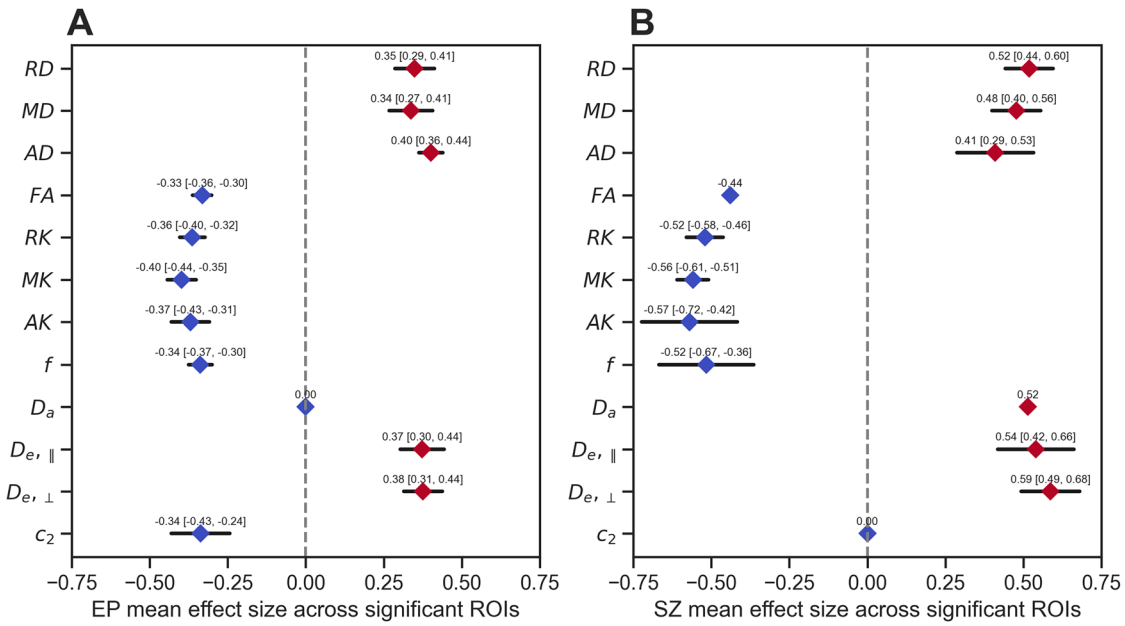

Fig. 4 Slightly modified to accomodate the request. Average effect sizes of significant ROIs for each dMRI metric in EP vs HC_{Young} (**A**) and SZ vs HC_{Old} (**B**). The black horizontal lines represent the confidence intervals.

biophysical models retain superior specificity in characterizing pathology.

Association between microstructure estimates, clinical characteristics and psychopathological symptom domains

We correlated clinical characteristics with microstructure in the WM core (i.e., averaged measure across all WM ROIs) because the diffusion MRI metrics showed widespread consistent changes across JHU ROIs in patients and strong effect sizes. Furthermore, this approach limits considerably the number of statistical tests. There were no significant associations between WM microstructure and age at psychosis onset, nor with illness duration (covaried with age). The intra-axonal diffusivity, D_a, showed significant negative association with CPZ-equivalent dose in the SZ group ($p_{FDR} = 0.013$), significantly different from the EP slope ($p_{FDR} = 0.0019$). To better understand the aging trajectories of WM microstructure in patients vs. HC we examined the interaction between age and the two grouping variables (EP + SZ) and HC, but no significant differences were found after FDR correction (Fig. S6). The associations between microstructure metrics in the WM core and symptom scores were also examined. Overall, correlations between psychiatric scales and WM microstructure metrics were stronger in SZ than EP and showed different cluster patterns between groups. However, no correlation survived FDR correction (Fig. S7).

DISCUSSION

With the present analysis, we studied a rich early psychosis and schizophrenia cohort (LSP), employing more advanced diffusion metrics than DTI, namely DKI and a comprehensive microstructure model, WMTI-W, both aimed at characterizing the WM pathology with increased sensitivity and specificity. We compared the patterns and effect sizes obtained from EP and SZ with the current literature as well as between the two patient groups. Finally, we tested the dMRI metrics against commonly used clinical measures and characteristics.

Our findings revealed that WM alterations are already present and widespread at the EP stage. We found a vast increase in diffusivities in both groups, especially in RD, and decrease in FA and kurtosis in the WM core, with large effect sizes. The increase in DTI diffusivities and decrease in FA confirm previous findings in similar cohorts [4, 8, 23, 71] and high effect sizes in the average WM [8]. The large effect sizes found for DKI metrics, particularly between SZ and HC_{Old}, support the added value of going beyond DTI in quantitative diffusion MRI analyses of clinical populations, as supported by several other patient studies [45, 50, 72] and animal models of disease [46, 47].

Regionally, the largest effect sizes were observed consistently in the ACR-R, but also in the PCR, the SLF, and the CC in EP. The corona radiata has often been reported to be affected in SZ, showing among the strongest regional effect sizes [8]. The CR collects fibers projecting from the cortex to the internal capsule, brainstem and thalamus [73] and is important for emotion, motivation, cognitive processing, and decision-making [74]. Specifically in SZ, reduced FA in the ACR was associated with impaired social cognition [75], and higher severity of auditory and verbal hallucinations [76]. The SLF is an association fiber that connects the frontal lobe to the rest of the ipsilateral brain, and whose FA increases significantly during normal development [77]. Reduced integrity of the SLF has previously been found in clinical high-risk subjects [78], recent-onset SZ [79], and was associated with reduced verbal fluency [79]. A recent meta-analysis of early-onset psychosis [6] (onset < 18 y.o.) and ultra high-risk individuals [26] reported both the SLF and PCR as the main affected ROIs, which contrasted findings in adults [8]. All the high effect size ROIs identified in early-onset and adult patients [6, 8] (SLF, PCR, ACR, CC) also showed the highest effect sizes in our LSP cohort.

We expected a good regional agreement between EP and SZ, which was confirmed by a high Dice score (0.36) and strong correlation between EP and SZ effect sizes. The regional agreement in effect sizes was particularly high for MD, MK ($r > 0.60$) and for $D_{e,\perp}$ ($r = 0.61$), suggesting higher sensitivity of these metrics at detecting shared regional alterations between early and late stages compared to the other metrics. These results indeed support the hypothesis that FA differences to HC originate during development and adolescence, remaining throughout the lifespan [23–26]. In this context, the widespread alterations found in EP could result from a shift in peaks in the WM development, achieved earlier in patients [4, 25] than HC, resulting in a persistent offset of the WM. However, it remains unclear from our data whether the WM alterations worsen with disease progression

towards chronic SZ, as effect sizes do become more pronounced in SZ but fewer ROIs are significantly different between SZ and HC_{Old}. Other studies, on the other hand, report worsening of the FA trajectories with age at later stages of the disease [4, 25, 80]. Our SZ cohort size is perhaps somewhat limited with respect to the wide age range, which could lower our statistics for this group.

Regarding agreement of the alterations found in the LSP cohort with the literature [8], we found an excellent agreement between FA effect sizes in ENIGMA vs both our EP and SZ cohorts ($r_{EP} = 0.47$, $r_{SZ} = 0.66$), indicating the patterns reported in ENIGMA are reproducible in different cohorts evaluated with different methodologies. Surprisingly, we found better agreement of ENIGMA MD and RD effect sizes with our MK and RK effect sizes ($r > 0.60$) rather than MD or RD ($0.26 < r < 0.41$). A possible explanation is that, in the simple DTI fit that does not estimate kurtosis jointly, the DTI metrics are biased by higher order features of the diffusion signal, i.e. kurtosis arising from the non-gaussian behavior of the water molecules. A full DKI fit improves the accuracy of DTI metrics while properly separating the non-gaussian effects in the kurtosis metrics (MK, RK, AK) [81]. In other words, ENIGMA DTI measures are influenced by a combination of gaussian and non-gaussian diffusion, while the LSP DTI measures are not, which could explain the better correlation between ENIGMA first-order measures (MD, RD) and LSP higher order measures (MK, RK).

When covarying the ROI diffusion measures with the matching core WM measures, only two ROIs remained significant: the PLIC in EP (increased MK, decreased MD) and ACR-R in SZ (increased MD). This result is consistent with ENIGMA [6, 8] previous findings in which only the PLIC (increased FA) survived the same type of analysis. This further confirms that despite the regional specificity, the alterations are driven by a common general effect across WM.

Moreover, the lack of significant associations of WM microstructure metrics with age at first psychosis, medication, duration of illness or symptomatology is also aligned with the literature [8, 82, 83]. Specifically, regarding symptomatology, the lack of associations could be explained by its transitory nature. The patient's symptomatologic state at the time of the MRI scan may differ from the state that led to the assigned clinical score. Furthermore, the difference in cluster patterns between the EP and SZ stages may be due to sampling variability and heterogeneity between the two cohorts rather than specific symptoms-microstructure relationships.

For the first time, we used WMTI-W, a comprehensive biophysical model of WM, to tease apart possible pathological contributions to the reported WM differences. Here, the effect sizes carried by the WMTI-W parameters were marginally lower than those by DTI or DKI. Nonetheless, the changes in model metrics improved the interpretation of WM changes in EP and SZ. Biophysical models come with improved specificity at a moderate cost in sensitivity [84]. For example, using a similar WM model in stroke showed preferential changes as increased f and dramatically decreased D_a, consistent with cytotoxic edema and beading [72], in multiple sclerosis as a decrease in f, fiber alignment, and higher extra-axonal diffusivities [72], consistent with demyelination, and in a rat model of Alzheimer's disease as a decrease in f and D_a, consistent with axonal injury and loss [49].

In EP and SZ, WMTI-W helps attribute the observed alterations to the extra-axonal compartment, due to the significant increase in $D_{e,\parallel}$ and $D_{e,\perp}$, and the lower axonal water fraction f. In validation studies, a similar – albeit more pronounced – pattern of alteration ($f \downarrow$, $D_{e,\parallel} \uparrow$, $D_{e,\perp} \uparrow$) has been shown to arise from demyelination, induced via chronic cuprizone intoxication in mice [46, 47, 85] (Table 1). Ultrastructural post-mortem studies in SZ reported myelinated WM fiber pathology in the form of decompacting and splitting of the myelin sheath and inclusions of vacuoles in-between myelin layers, small-axons atrophy, and the presence of swollen or dystrophic oligodendroglia [11–13], all of which can explain the demyelination-like pattern drawn by $D_{e,\parallel}$, $D_{e,\perp}$ and f. In the SZ group, the WM core analysis also suggested higher intra-axonal diffusivity, D_a, in this group, but only two specific ROIs sustained this trend (CING and CC).

Previous works using NODDI [34], a comparable but more constrained biophysical model, also reported reduced neurite density (comparable to f) in several ROIs, and increased orientation dispersion index (corresponding to lower c_2) in both first episode and chronic SZ [86]. These patterns of preferentially altered extra-axonal environment are also consistent with reports of global increase in "free water" using the FWI technique in SZ cohorts [35], although FWI conflates potential pathological mechanisms by defining a tissue compartment (intra- and extra-axonal) vs a free water (CSF) one.

Limitations

The first two main limitations of the present study are the use of the age-range approach instead of age-matching and the use of data from two scanners, which is a source of bias, possibly even after careful harmonization. The age-range approach was preferred to maintain the sample size as large as possible to better correct for the scanner effect and increase the statistical power of the analyses. In addition, we believe it was preferable not to pair participants by age at the cost of pairing data from different scanners, which could introduce more bias. With regard to the WM biophysical model, the modeling of the axonal dispersion as Watson distribution is not ideally suited for multi-fiber configurations, e.g. crossing fibers [16]. Finally, while the subject numbers in the cohort are sufficiently high to support our conclusions, they are not balanced between groups, which is due to the concrete challenge in recruiting EP and SZ patients. In the light of these limitations, the generalizability of our conclusions needs to be confirmed in other cohorts.

CONCLUSIONS

In conclusion, with this work we confirmed that WM alterations are already present in the early psychosis stages, consistent with shifted maturation, and are more widespread in EP, but more pronounced in SZ. The regional alterations of higher DTI diffusivities and lower kurtosis found in our cohort matched the DTI patterns found in ENIGMA-schizophrenia. WMTI-W model parameters indicate that the WM alterations in patients manifest preferentially perpendicular to the axons as extra-cellular increase in diffusivities, decreased intra-cellular water fraction, and loss of fiber alignment, consistent with early myelin aberrations. The direct link between WM alterations and symptomatology is, however, limited.

DATA AVAILABILITY

The data supporting the findings of this study are available from the corresponding author upon reasonable request. The code can be found here: *github.com/Mic-map/WMTI-Watson_Python*.

REFERENCES

1. Wittchen HU, Jacobi F, Rehm J, Gustavsson A, Svensson M, Jönsson B, et al. The size and burden of mental disorders and other disorders of the brain in Europe 2010. Eur Neuropsychopharmacol J Eur Coll Neuropsychopharmacol. 2011;21:655–79.
2. Keshavan MS, Berger G, Zipursky RB, Pantelis C, Wood SJ, Pantelis C. Neurobiology of early psychosis. Br J Psychiatry. 2005;187:s8–s18.
3. Harrison PJ. The neuropathology of schizophrenia: a critical review of the data and their interpretation. Brain. 1999;122:593–624.
4. Cetin-Karayumak S, Di Biase MA, Chunga N, Reid B, Somes N, Lyall AE, et al. White matter abnormalities across the lifespan of schizophrenia: a harmonized multi-site diffusion MRI study. Mol Psychiatry. 2020;25:3208–19.
5. Friedman Joseph I, Tang C, Carpenter D, Buchsbaum M, Schmeidler J, Flanagan L, et al. Diffusion tensor imaging findings in first-episode and chronic schizophrenia patients. Am J Psychiatry. 2008;165:1024–32.

6. Barth C, Kelly S, Nerland S, Jahanshad N, Alloza C, Ambrogi S, et al. In vivo white matter microstructure in adolescents with early-onset psychosis: a multi-site mega-analysis. Mol Psychiatry. 2023;28:1159–69.
7. Karlsgodt KH. White matter microstructure across the psychosis spectrum. Trends Neurosci. 2020;43:406–16.
8. Kelly S, Jahanshad N, Zalesky A, Kochunov P, Agartz I, Alloza C, et al. Widespread white matter microstructural differences in schizophrenia across 4322 individuals: results from the ENIGMA Schizophrenia DTI Working Group. Mol Psychiatry. 2018;23:1261–9.
9. van Velzen LS, Kelly S, Isaev D, Aleman A, Aftanas LI, Bauer J, et al. White matter disturbances in major depressive disorder: a coordinated analysis across 20 international cohorts in the ENIGMA MDD working group. Mol Psychiatry. 2020;25:1511–25.
10. Hof PR, Haroutunian V, Friedrich VL, Byne W, Buitron C, Perl DP, et al. Loss and altered spatial distribution of oligodendrocytes in the superior frontal gyrus in schizophrenia. Biol Psychiatry. 2003;53:1075–85.
11. Uranova NA, Vikhreva OV, Rachmanova VI, Orlovskaya DD. Ultrastructural alterations of myelinated fibers and oligodendrocytes in the prefrontal cortex in schizophrenia: a postmortem morphometric study. Schizophr Res Treat. 2011;2011:e325789.
12. Uranova NA, Vikhreva OV, Rakhmanova VI, Orlovskaya DD. Ultrastructural pathology of oligodendrocytes adjacent to microglia in prefrontal white matter in schizophrenia. Npj Schizophr. 2018;4:1–10.
13. Williams M (ed.). *The Neuropathology of Schizophrenia*. Cham: Springer International Publishing, 2021 https://doi.org/10.1007/978-3-030-68308-5.
14. Uranova NA, Vikhreva OV, Rakhmanova VI, Orlovskaya DD Dystrophy of oligodendrocytes and adjacent microglia in prefrontal gray matter in schizophrenia. *Front Psychiatry* 2020; 11. https://www.frontiersin.org/articles/10.3389/fpsyt.2020.00204 (accessed 10 Mar 2023).
15. Beaulieu C. The basis of anisotropic water diffusion in the nervous system - a technical review. NMR Biomed. 2002;15:435–55.
16. Jelescu IO, Budde MD Design and validation of diffusion MRI models of white matter. *Front Phys* 2017; 5. https://www.frontiersin.org/articles/10.3389/fphy.2017.00061 (accessed 1 Dec2022).
17. Le Bihan D, Mangin J-F, Poupon C, Clark CA, Pappata S, Molko N, et al. Diffusion tensor imaging: concepts and applications. J Magn Reson Imaging. 2001;13:534–46.
18. Dwork AJ, Mancevski B, Rosoklija G. White matter and cognitive function in schizophrenia. Int J Neuropsychopharmacol. 2007;10:513.
19. Pasternak O, Westin C-F, Dahlben B, Bouix S, Kubicki M. The extent of diffusion MRI markers of neuroinflammation and white matter deterioration in chronic schizophrenia. Schizophr Res. 2015;161:113–8.
20. Klauser P, Baker ST, Cropley VL, Bousman C, Fornito A, Cocchi L, et al. White matter disruptions in schizophrenia are spatially widespread and topologically converge on brain network hubs. Schizophr Bull. 2017;43:425–35.
21. Kraguljac NV, McDonald WM, Widge AS, Rodriguez CI, Tohen M, Nemeroff CB. Neuroimaging biomarkers in schizophrenia. Am J Psychiatry. 2021;178:509–21.
22. Kochunov P, Hong LE, Dennis EL, Morey RA, Tate DF, Wilde EA, et al. ENIGMA-DTI: Translating reproducible white matter deficits into personalized vulnerability metrics in cross-diagnostic psychiatric research. Hum Brain Mapp. 2020;43:194.
23. Samartzis L, Dima D, Fusar-Poli P, Kyriakopoulos M. white matter alterations in early stages of schizophrenia: a systematic review of diffusion tensor imaging studies. J Neuroimaging. 2014;24:101–10.
24. Peters BD, Karlsgodt KH. White matter development in the early stages of psychosis. Schizophr Res. 2015;161:61–69.
25. Kochunov P, Hong LE. Neurodevelopmental and neurodegenerative models of schizophrenia: white matter at the center stage. Schizophr Bull. 2014;40:721–8.
26. Carletti F, Woolley JB, Bhattacharyya S, Perez-Iglesias R, Fusar Poli P, Valmaggia L, et al. Alterations in white matter evident before the onset of psychosis. Schizophr Bull. 2012;38:1170–9.
27. Jensen JH, Helpern JA, Ramani A, Lu H, Kaczynski K. Diffusional kurtosis imaging: The quantification of non-gaussian water diffusion by means of magnetic resonance imaging. Magn Reson Med. 2005;53:1432–40.
28. Jensen JH, Helpern JA. MRI quantification of non-Gaussian water diffusion by kurtosis analysis. NMR Biomed. 2010;23:698–710.
29. Narita H, Tha KK, Hashimoto N, Hamaguchi H, Nakagawa S, Shirato H, et al. Mean kurtosis alterations of cerebral white matter in patients with schizophrenia revealed by diffusion kurtosis imaging. Prog Neuropsychopharmacol Biol Psychiatry. 2016;71:169–75.
30. Zhu J, Zhuo C, Qin W, Wang D, Ma X, Zhou Y, et al. Performances of diffusion kurtosis imaging and diffusion tensor imaging in detecting white matter abnormality in schizophrenia. NeuroImage Clin. 2015;7:170–6.
31. Zhang F, Cho KIK, Tang Y, Zhang T, Kelly S, Biase MD, et al. MK-Curve improves sensitivity to identify white matter alterations in clinical high risk for psychosis. NeuroImage. 2021;226:117564.
32. Kochunov P, Rowland LM, Fieremans E, Veraart J, Jahanshad N, Eskandar G, et al. Diffusion-weighted imaging uncovers likely sources of processing-speed deficits in schizophrenia. Proc Natl Acad Sci. 2016;113:13504–9.
33. Pasternak O, Sochen N, Gur Y, Intrator N, Assaf Y. Free water elimination and mapping from diffusion MRI. Magn Reson Med. 2009;62:717–30.
34. Zhang H, Schneider T, Wheeler-Kingshott CA, Alexander DC. NODDI: practical in vivo neurite orientation dispersion and density imaging of the human brain. NeuroImage. 2012;61:1000–16.
35. Carreira Figueiredo I, Borgan F, Pasternak O, Turkheimer FE, Howes OD. White-matter free-water diffusion MRI in schizophrenia: a systematic review and meta-analysis. Neuropsychopharmacology. 2022;47:1413–20.
36. Cetin-Karayumak S, Lyall AE, Di Biase MA, Seitz-Holland J, Zhang F, Kelly S et al. Characterization of the extracellular free water signal in schizophrenia using multi-site diffusion MRI harmonization. Mol Psychiatry. 2023;28:2030–8.
37. Rae CL, Davies G, Garfinkel SN, Gabel MC, Dowell NG, Cercignani M, et al. Deficits in neurite density underlie white matter structure abnormalities in first-episode psychosis. Biol Psychiatry. 2017;82:716–25.
38. Kraguljac NV, Anthony T, Morgan CJ, Jindal RD, Burger MS, Lahti AC. White matter integrity, duration of untreated psychosis, and antipsychotic treatment response in medication-naïve first-episode psychosis patients. Mol Psychiatry. 2021;26:5347–56.
39. Kraguljac NV, Anthony T, Monroe WS, Skidmore FM, Morgan CJ, White DM, et al. A longitudinal neurite and free water imaging study in patients with a schizophrenia spectrum disorder. Neuropsychopharmacology. 2019;44:1932–9.
40. Novikov DS, Kiselev VG, Jespersen SN. On modeling. Magn Reson Med. 2018;79:3172–93.
41. Jelescu IO, Veraart J, Fieremans E, Novikov DS. Degeneracy in model parameter estimation for multi-compartmental diffusion in neuronal tissue. NMR Biomed. 2016;29:33–47.
42. Jespersen SN, Olesen JL, Hansen B, Shemesh N. Diffusion time dependence of microstructural parameters in fixed spinal cord. NeuroImage. 2018;182:329–42.
43. Fieremans E, Jensen JH, Helpern JA. White matter characterization with diffusional kurtosis imaging. NeuroImage. 2011;58:177–88.
44. Jelescu IO, Fieremans E Chapter 2 - Sensitivity and specificity of diffusion MRI to neuroinflammatory processes. In: Laule C, Port JD (eds). *Advances in Magnetic Resonance Technology and Applications*. Academic Press, 2023, pp 31–50.
45. Kamiya K, Hori M, Irie R, Miyajima M, Nakajima M, Kamagata K, et al. Diffusion imaging of reversible and irreversible microstructural changes within the corticospinal tract in idiopathic normal pressure hydrocephalus. NeuroImage Clin. 2017;14:663–71.
46. Guglielmetti C, Veraart J, Roelant E, Mai Z, Daans J, Van Audekerke J, et al. Diffusion kurtosis imaging probes cortical alterations and white matter pathology following cuprizone induced demyelination and spontaneous remyelination. NeuroImage. 2016;125:363–77.
47. Jelescu IO, Zurek M, Winters KV, Veraart J, Rajaratnam A, Kim NS, et al. In vivo quantification of demyelination and recovery using compartment-specific diffusion MRI metrics validated by electron microscopy. NeuroImage. 2016;132:104–14.
48. Dong JW, Jelescu IO, Ades-Aron B, Novikov DS, Friedman K, Babb JS, et al. Diffusion MRI biomarkers of white matter microstructure vary nonmonotonically with increasing cerebral amyloid deposition. Neurobiol Aging. 2020;89:118–28.
49. Tristão Pereira C, Diao Y, Yin T, da Silva AR, Lanz B, Pierzchala K, et al. Synchronous nonmonotonic changes in functional connectivity and white matter integrity in a rat model of sporadic Alzheimer's disease. NeuroImage. 2021;225:117498.
50. Pavan T, Ribaldi F, Pievani M, Jovicich J, Garibotto V, Frisoni GB, et al. Microstructure of white matter, probed with diffusion MRI modeling, reveals distinct correlations between intra- vs extra-cellular spaces and Tau Load. Alzheimers Dement. 2023;19:e078259.
51. Chung S, Fieremans E, Wang X, Kucukboyaci NE, Morton CJ, Babb J, et al. White matter tract integrity: an indicator of axonal pathology after mild traumatic brain injury. J Neurotrauma. 2018;35:1015–20.
52. Yung AR, Yuen HP, McGorry PD, Phillips LJ, Kelly D, Dell'Olio M, et al. Mapping the onset of psychosis: the comprehensive assessment of at-risk mental states. Aust N Z J Psychiatry. 2005;39:964–71.
53. Tustison NJ, Avants BB, Cook PA, Zheng Y, Egan A, Yushkevich PA, et al. N4ITK: improved N3 bias correction. IEEE Trans Med Imaging. 2010;29:1310–20.
54. Avants BB, Epstein CL, Grossman M, Gee JC. Symmetric diffeomorphic image registration with cross-correlation: evaluating automated labeling of elderly and neurodegenerative brain. Med Image Anal. 2008;12:26–41.
55. Ades-Aron B, Veraart J, Kochunov P, McGuire S, Sherman P, Kellner E, et al. Evaluation of the accuracy and precision of the diffusion parameter EStImation with Gibbs and NoisE removal pipeline. NeuroImage. 2018;183:532–43.
56. Veraart J, Sijbers J, Sunaert S, Leemans A, Jeurissen B. Weighted linear least squares estimation of diffusion MRI parameters: Strengths, limitations, and pitfalls. NeuroImage. 2013;81:335–46.
57. Mori S, Wakana S, Van Zijl PC, Nagae-Poetscher LM. MRI atlas of human white matter. Elsevier; 2005.

58. Smith SM, Jenkinson M, Johansen-Berg H, Rueckert D, Nichols TE, Mackay CE, et al. Tract-based spatial statistics: voxelwise analysis of multi-subject diffusion data. NeuroImage. 2006;31:1487–505.
59. Zalesky A. Moderating registration misalignment in voxelwise comparisons of DTI data: a performance evaluation of skeleton projection. Magn Reson Imaging. 2011;29:111–25.
60. Schwarz CG, Reid RI, Gunter JL, Senjem ML, Przybelski SA, Zuk SM, et al. Improved DTI registration allows voxel-based analysis that outperforms Tract-Based Spatial Statistics. NeuroImage. 2014;94:65–78.
61. Pinheiro AP, Johnson JF, Amorim M, Roberto M, Schwartze M, Kotz SA, et al. The cerebellum links to positive symptoms of psychosis: a systematic review and meta-analysis. Schizophr Bull Open. 2021;2:sgab039.
62. American Psychiatric Association. *Diagnostic and Statistical Manual of Mental Disorders (4th ed., text rev.)*. 2000.
63. Kay SR, Fiszbein A, Opler LA. The positive and negative syndrome scale (PANSS) for schizophrenia. Schizophr Bull. 1987;13:261–76.
64. Montgomery SA, Asberg M. A new depression scale designed to be sensitive to change. Br J Psychiatry J Ment Sci. 1979;134:382–9.
65. Wallwork RS, Fortgang R, Hashimoto R, Weinberger DR, Dickinson D. Searching for a consensus five-factor model of the Positive and Negative Syndrome Scale for schizophrenia. Schizophr Res. 2012;137:246–50.
66. Fortin J-P, Parker D, Tunç B, Watanabe T, Elliott MA, Ruparel K, et al. Harmonization of multi-site diffusion tensor imaging data. NeuroImage. 2017;161:149–70.
67. Alemán-Gómez Y, Najdenovska E, Roine T, Fartaria MJ, Canales-Rodríguez EJ, Rovó Z, et al. Partial-volume modeling reveals reduced gray matter in specific thalamic nuclei early in the time course of psychosis and chronic schizophrenia. Hum Brain Mapp. 2020;41:4041–61.
68. Brunner E, Munzel U. The nonparametric behrens-fisher problem: asymptotic theory and a small-sample approximation. Biom J. 2000;42:17–25.
69. Karch JD. Psychologists should use Brunner-Munzel's instead of Mann-Whitney's U test as the default nonparametric procedure. Adv Methods Pract Psychol Sci. 2021;4:2515245921999602.
70. R Core Team. *R: A Language and Environment for Statistical Computing*. R Foundation for Statistical Computing: Vienna, Austria, 2023 https://www.R-project.org/.
71. Tamnes CK, Agartz I. White matter microstructure in early-onset schizophrenia: a systematic review of diffusion tensor imaging studies. J Am Acad Child Adolesc Psychiatry. 2016;55:269–79.
72. Liao Y, Coelho S, Chen J, Ades-Aron B, Pang M, Stepanov V, et al. Mapping tissue microstructure of brain white matter in vivo in health and disease using diffusion MRI. Imaging Neurosci. 2024;2:1–17.
73. Yakar F, Eroglu U, Peker E, Armagan E, Comert A, Ugur HC. Structure of corona radiata and tapetum fibers in ventricular surgery. J Clin Neurosci. 2018;57:143–8.
74. Safadi Z, Grisot G, Jbabdi S, Behrens TE, Heilbronner SR, McLaughlin NC, et al. Functional segmentation of the anterior limb of the internal capsule: linking white matter abnormalities to specific connections. J Neurosci. 2018;38:2106.
75. Burke T, Holleran L, Mothersill D, Lyons J, O'Rourke N, Gleeson C, et al. Bilateral anterior corona radiata microstructure organisation relates to impaired social cognition in schizophrenia. Schizophr Res. 2023;262:87–94.
76. Ćurčić-Blake B, Nanetti L, van der Meer L, Cerliani L, Renken R, Pijnenborg GHM, et al. Not on speaking terms: hallucinations and structural network disconnectivity in schizophrenia. Brain Struct Funct. 2015;220:407–18.
77. Peters BD, Szeszko PR, Radua J, Ikuta T, Gruner P, DeRosse P, et al. White matter development in adolescence: diffusion tensor imaging and meta-analytic results. Schizophr Bull. 2012;38:1308–17.
78. Tang Y, Pasternak O, Kubicki M, Rathi Y, Zhang T, Wang J, et al. Altered cellular white matter but not extracellular free water on diffusion MRI in individuals at clinical high risk for psychosis. Am J Psychiatry. 2019;176:820–8.
79. Karlsgodt KH, van Erp TGM, Poldrack RA, Bearden CE, Nuechterlein KH, Cannon TD. Diffusion tensor imaging of the superior longitudinal fasciculus and working memory in recent-onset schizophrenia. Biol Psychiatry. 2008;63:512–8.
80. Cropley VL, Klauser P, Lenroot RK, Bruggemann J, Sundram S, Bousman C, et al. Accelerated gray and white matter deterioration with age in schizophrenia. Am J Psychiatry. 2017;174:286–95.
81. Veraart J, Poot DHJ, Van Hecke W, Blockx I, Van der Linden A, Verhoye M, et al. More accurate estimation of diffusion tensor parameters using diffusion kurtosis imaging. Magn Reson Med. 2011;65:138–45.
82. Kanaan R, Barker G, Brammer M, Giampietro V, Shergill S, Woolley J, et al. White matter microstructure in schizophrenia: effects of disorder, duration and medication. Br J Psychiatry. 2009;194:236–42.
83. Di Biase MA, Cetin-Karayumak S, Lyall AE, Zalesky A, Cho KIK, Zhang F, et al. White matter changes in psychosis risk relate to development and are not impacted by the transition to psychosis. Mol Psychiatry. 2021;26:6833–44.
84. Jelescu IO, Palombo M, Bagnato F, Schilling KG. Challenges for biophysical modeling of microstructure. J Neurosci Methods. 2020;344:108861.
85. Falangola MF, Guilfoyle DN, Tabesh A, Hui ES, Nie X, Jensen JH, et al. Histological correlation of diffusional kurtosis and white matter modeling metrics in cuprizone-induced corpus callosum demyelination. NMR Biomed. 2014;27:948–57.
86. Kraguljac NV, Guerreri M, Strickland MJ, Zhang H. Neurite orientation dispersion and density imaging in psychiatric disorders: a systematic literature review and a technical note. Biol Psychiatry Glob Open Sci. 2023;3:10–21.
87. Zhuo J, Xu S, Proctor JL, Mullins RJ, Simon JZ, Fiskum G, et al. Diffusion kurtosis as an in vivo imaging marker for reactive astrogliosis in traumatic brain injury. NeuroImage. 2012;59:467–77.
88. Budde MD, Frank JA. Neurite beading is sufficient to decrease the apparent diffusion coefficient after ischemic stroke. Proc Natl Acad Sci. 2010;107:14472–7.
89. Lee H-H, Papaioannou A, Kim S-L, Novikov DS, Fieremans E. A time-dependent diffusion MRI signature of axon caliber variations and beading. Commun Biol. 2020;3:1–13.
90. Wang Y, Wang Q, Haldar JP, Yeh F-C, Xie M, Sun P, et al. Quantification of increased cellularity during inflammatory demyelination. Brain. 2011;134:3590–601.

ACKNOWLEDGEMENTS

This work was supported by the Swiss National Science Foundation (PCEFP2_194260, to I.J.), the National Center of Competence in Research (NCCR) "SYNAPSY - The Synaptic Bases of Mental Diseases" from the Swiss National Science Foundation (n° 51NF40 – 185897 to KQD & PC) and the Foundation Alamaya. LA is supported by Carigest fellowship. PK, DD and LA are supported by the Adrian & Simone Frutiger Foundation.

AUTHOR CONTRIBUTIONS

Conceptualization: TP, PS, PK, IJ; Data Acquisition: MC; Data curation: TP, YA, RJ; Analysis: TP; Supervision: PS, PK, IJ; Writing – original draft: TP, IJ; Writing – review & editing: All authors.

COMPETING INTERESTS

The authors declare no competing interests.

ETHICS APPROVAL AND CONSENT TO PARTICIPATE

The study was approved by the local Ethics Committee of the Canton of Vaud (CER-VD 382/11 and 2018-01731, Switzerland) and performed in accordance with the relevant guidelines and regulations. All participants provided their informed consent to take part in the study.

ADDITIONAL INFORMATION

Supplementary information The online version contains supplementary material available at https://doi.org/10.1038/s41398-025-03397-1.

Correspondence and requests for materials should be addressed to Tommaso Pavan.

Reprints and permission information is available at http://www.nature.com/reprints

Publisher's note Springer Nature remains neutral with regard to jurisdictional claims in published maps and institutional affiliations.